Theoretical and Experimental Analysis of a Micro Turbojet Engine's Performance

Aly M. Elzahaby, Mohamed K. Khalil, Hesham E. Khalil

Abstract— A micro turbojet engine is modeled using energy and momentum equations, which are solved to predict its performance and the flow parameters across it at design conditions. In order to simulate the engine's performance at off-design conditions, the complete performance maps of the different engine components are required. Therefore, empirical equations are used to predict the maps of the compressor and the combustion chamber, and then the off-design engine performance is obtained. The model results are compared with the results of a commercial software and verified with the experimental results. The analytical model predicts the experimental performance of the engine successfully (Thrust and fuel consumption), and it is proved to be more accurate than the used commercial software. The model's accuracy can be increased furthermore if there is more data available about the turbine performance map. The engine used in this study is mounted with a load cell to measure its net thrust and a fuel flow meter to measure its fuel consumption. It was already mounted with a temperature sensor at the exhaust and a rotational speed sensor. The variation of these parameters is monitored across its speed range of 33,000 to 112,000 rpm.

Index Terms— ANSYS CFX, Combustion chamber, EES, Equilbrium run curves, Gasturb, Radial compressor performance, Micro turbojet.

1 Introduction

Recently, during the last decade, micro turbojet engines gained a lot of popularity among airplane enthusiasts and young researchers due to its simple design, low cost and easy operability. These small engines can be installed in small laboratories without the need to any expensive infrastructure. One of the most important applications of the micro turbojet engines is being the propulsive power source for Unmanned Aerial Vehicles (UAV's). Its high power to weight ratio is the main reason for that, even with its high specific fuel consumption (SFC) relative to commercial turbojet engines.

Previous studies were conducted on several micro turbojet engines' models, to measure their performance experimentally and predict it theoretically using CFD and/or analytical models [1], [2], [3], [4], [5], [6], [7], [8], [9], [10], [11], [12], [13]. Some of these studies used map-scaling to predict the performance variation of the compressor at different speeds [1], [2], [3]. Other studies used CFD analysis and commercial software to predict it [2], [4], [5], [6], [7], [8].

This paper is conducted on studying micro turbojet engines' performance by predicting it theoretically and verifying this prediction experimentally.

2 Engine Specifications

The engine used in this study has a rated thrust of 230 N at 112,000 rpm, and its complete technical specifications are given in Table 1.

- *Aly M. Elzahaby. Mechanical power engineering department, Tanta University, Egypt. E-mail: elzahaby47@gmail.com*
- *Mohamed K. Khalil. MTC, Egypt. E-mail: khilo99@yahoo.com*
- *Hesham Elagmy Khalil. Mechanical engineering department, Kafrelsheikh University, Egypt. E-mail: hisham_khalil2011@eng.kfs.edu.eg (Corresponding author)*

This is a single spool turbojet engine with a single stage radial compressor and a single stage radial turbine followed by an exhaust convergent nozzle. The engine was provided with a rotational speed sensor and a temperature sensor at the exhaust nozzle. Fig. 1 shows the engine longitudinal section showing the main studied stations through the engine.

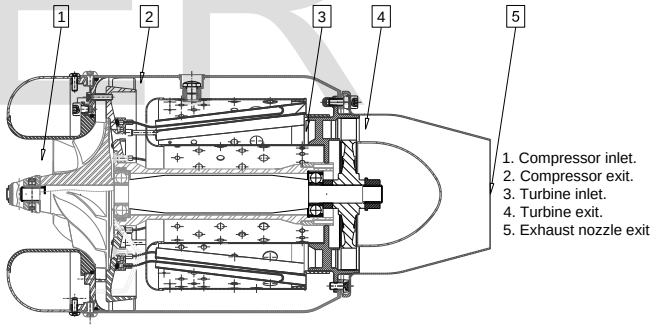

Fig. 1 longitudinal section of the engine with its different stations.

TABLE 1 TECHNICAL ENGINE'S SPECIFICATIONS AS PROVIDED FROM THE MANUFACTURER

Parameter	Value
Compressor pressure ratio (π_{ct})	3.7
Idle thrust	9 N
Maximum thrust	230 N
Idle speed	33,000 rpm
Maximum speed	112,000 rpm
Maximum Exhaust Gas Temperature (EGT)	750°C
Mass flow rate	0.45 kg/s
Maximum exhaust velocity	1,840 km/hr
Maximum fuel consumption	0.584 kg/min
Fuel mixture (By volume)	95% Jet-A1+ 5% Mobil jet oil 254

3 Engine Components' Modeling at Design

CONDITION

A complete thermodynamic cycle analysis of the engine at stand conditions is simulated using a computer software Engineering Equation Solver (EES). EES has the capability to solve up to 12,000 equations in a time-efficient manner and has a large library of the thermo-physical properties of most popular fluids.

Some of the specifications of the engine's components and their performance maps are not provided by the manufacturer, therefore in order to solve the thermodynamic cycle at design conditions, an iterative process is implemented using the engines' known parameters (Thrust, air flow rate and EGT) until convergence is reached.

3.1 Air properties

Air is assumed at standard conditions of 288 K and 101,325 Pa at the inlet of the engine. Its specific heat capacity at constant pressure and specific heat ratio are assumed constants, and equal to 1,005 J/kg.K and 1.4, respectively.

3.2 Combustion gases' properties

The fuel used with this engine is Jet-A1. Its chemical composition contains approximately 15% hydrogen and 85% carbon by weight. These ratios are based on approximating it as kerosene fuel [9]. Knowing the amount of air required for the combustion process and the excess air ratio, the chemical composition of combustion gases is calculated.

Excess air ratio is assumed within an acceptable range (2.5 to 3.5) and after multiple iterations; its value converged to 2.861 at design conditions.

Specific heat capacities of the gases' mixture are calculated according to governing equations of ideal gases mixtures [15] shown in (1) & (2), which y_i is the molar fraction of each gas component, c_p is the specific heat capacity at constant pressure and M is the molar mass.

$$c_p' = \sum y_i \, c_{p_i} \tag{1}$$

$$M' = \frac{1}{\sum y_i M_i} \tag{2}$$

Specific heat capacities vary from the combustion chamber exit until reaching the engine's exhaust due to temperature drop at this region and the temperature effect on each component of the exhaust gases mixture. Their values are calculated at both locations and an average value is computed. Fig. 2 shows the variation of these values across the engine operating regimes, and prove that using the average value at each operating point generates an acceptable error less than 1.3%.

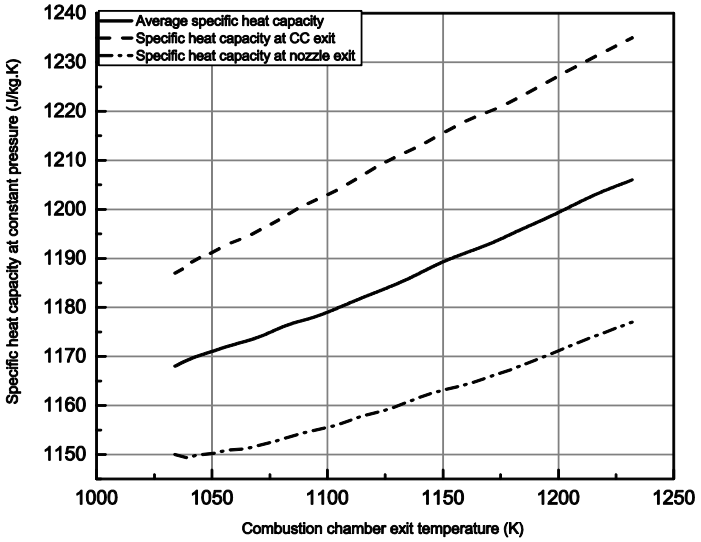

Fig. 2 Variation of specific heat capacity at constant pressure for combustion gases with temperature and their deviation from average value.

3.3 Engine's inlet

Airflow in the inlet section is assumed adiabatic with an average constant total pressure recovery factor (σ_{in}) equals to 0.96 [16].

$$\sigma_{in} = \frac{P_{1_t}}{P_{0_t}} \tag{3}$$

3.4 Compressor

Airflow through the compressor is assumed adiabatic [3]. Unfortunately, compressor's performance map is not available, so the compressor's total adiabatic efficiency (η_{c_t}) is iterated until reaching a convergent solution of 72.76%.

$$\left(\frac{T_{2_{t_{ad}}}}{T_{1_t}}\right)^{\gamma} = \pi_{c_t}^{\gamma-1} \tag{4}$$

$$\eta_{c_t} = \frac{T_{2_{t_{ad}}} - T_{1_t}}{T_{2_t} - T_{1_t}} \tag{5}$$

$$w_c = c_p(T_{2_t} - T_{1_t}) \tag{6}$$

3.5 Combustion chamber

The combustion process is assumed to end completely before entering the turbine. Total pressure recovery factor across the combustion chamber (σ_{cc}) is assumed within an acceptable range 0.93 to 0.97 at design condition [16].

$$\sigma_{cc} = \frac{P_{3_t}}{P_{2_t}} \tag{7}$$

Energy losses due to imperfect burning at design condition is represented by a burning efficiency of 95%, according to other micro turbojet engines with similar output power [11]. In addition, the increase in mass flowrate at the combustor exit is neglected to simplify the solving process and reduce its computing time.

$$\eta_{cc} = \frac{\dot{m}_a(c_p' T_{3_t} - c_p T_{2_t})}{\dot{m}_f LHV} \tag{8}$$

The superscript of c_p' refers to the properties of the combustion gases.

3.6 Turbine

Flow through the turbine is assumed adiabatic [3] with a total adiabatic efficiency of 89% similar to a same category micro turbojet engine [11].

$$\left(\frac{T_{4_{t_{ad}}}}{T_{1_t}}\right)^{\gamma} = \pi_{T_t}^{\gamma-1} \quad (9)$$

$$\eta_{T_t} = \frac{T_{3_t} - T_{4_t}}{T_{3_t} - T_{4_{t_{ad}}}} \quad (10)$$

$$w_t = c_p'(T_{3_t} - T_{4_t}) \quad (11)$$

Power generated by the turbine is consumed completely to power the compressor and overcome mechanical losses between them. Equation (12) shows the energy balance between these two components.

$$w_c = \eta_{mech} w_T \quad (12)$$

3.7 Exhaust nozzle

Because of the low compression ratio of the engine, the exhaust nozzle is estimated as unchoked. This result is similar to the case of using SR-30 micro turbojet engine [4]. In addition, after solving the governing equation of the entire engine, the flow rate is found lower than the choked flow rate of the exhaust nozzle.

$$\dot{m}_a = \frac{A_{EN} C_{d_{EN}} P_{4_t}}{R' T_{4_t}} \sqrt{2c_p' T_{4_t}\left(\left(\frac{P_0}{P_{4_t}}\right)^{\frac{2}{\gamma'}} - \left(\frac{P_0}{P_{4_t}}\right)^{\frac{\gamma'+1}{\gamma'}}\right)} \quad (13)$$

$$C_5 = \sqrt{2c_p' \eta_{EN} T_{4_t}\left(1 - \left(\frac{P_0}{P_{4_t}}\right)^{\frac{\gamma'-1}{\gamma'}}\right)} \quad (14)$$

After solving this set of equations, the full parameters of the engine at design speed are reached. The exhaust nozzle area required to achieve the stated performance by the Original Equipment Manufacturer (OEM) is found to be 23.85 cm^2, while the actual nozzle mounted to the engine has an exhaust area of 27.1 cm^2 with an increase of 13.6%. This wider nozzle is used for securer operation, lower engine's temperatures and larger stall-free operating regime of the engine.

4 Off-design condition

4.1 Compressor map

The compressor map is generated based on empirical formulas, curve fitting equations and figures [16] used previously to predict the performance map of large-scale radial compressors for speed range of 72% to 103% of design speed.

First, the relative axial velocities $\hat{C}_a'$ at surge line for different relative speeds $0.73 < \bar{n} < 1.1$ are calculated from (15).

$$\hat{C}_a' = 0.6786 \times \bar{n} + 0.2316 \quad (15)$$

The relative parameters at the surge point for design speed (w'/w_{des} & η'/η_{des}) are calculated as a function of relative axial flow velocity $\hat{C}_a'$ from Figs. 3 & 4. Consequently, the surge compression ratio and mass flow rate at design speed $\bar{n} = 1$ are calculated from (16) & (17).

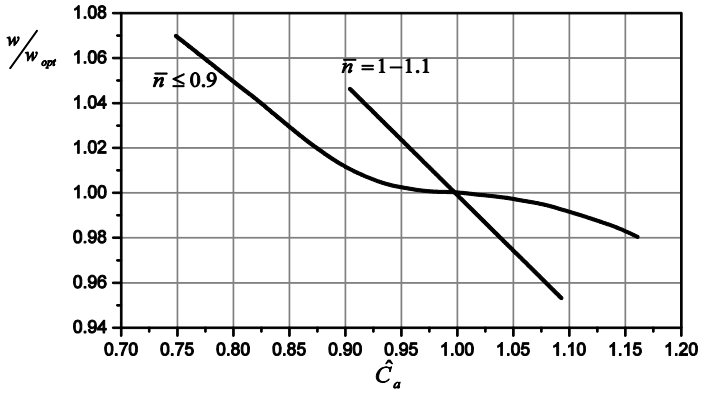

Fig. 3 The Ratio between compressor work and its optimum value at any relative speed $\bar{n}$, as a function of relative axial velocity $\hat{C}_a$ [16].

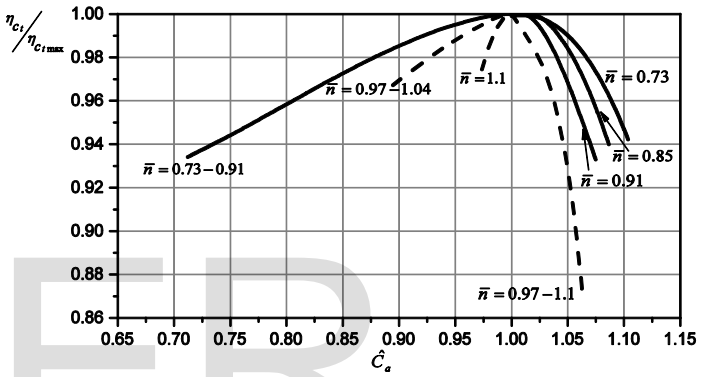

Fig. 4 Ratio between compressor total efficiency and its maximum value as a function of relative axial velocity $\hat{C}_a$ [16].

$$\pi_{c_t}' = \left(1 + \frac{w_{c_t}'}{w_{c_{t_{opt}}}} \frac{\eta_{c_t}'}{\eta_{c_{t_{max}}}} \left(\pi_{c_{t_{des}}}^{\frac{\gamma-1}{\gamma}} - 1\right)\right)^{\frac{\gamma}{\gamma-1}} \quad (16)$$

$$\dot{m}_{\bar{n}=1}' = \hat{C}_a' \dot{m}_{des} \sqrt[3]{\frac{\pi_{c_t}'}{\pi_{c_{t_{des}}}}} \quad (17)$$

For different operating speeds, the efficiency ratio $\eta_{ct}'/\eta_{ct_{\bar{n}=1}}'$ at the surge line is calculated from (18), and then both the compression ratios and flow rates at surge line are calculated from (19) & (20), which are enough data to plot the compressor's surge line.

$$\eta_{c_t}'/\eta_{c_{t_{\bar{n}=1}}}' = 168.49\bar{n}^6 - 870.35\bar{n}^5 + 1855\bar{n}^4 - 2089.6\bar{n}^3 + 1313\bar{n}^2 - 436.43\bar{n} + 60.924 \quad (18)$$

$$\pi_{c_t}' = \left(1 + \left(\pi_{c_{t_{\bar{n}=1}}}^{\frac{\gamma-1}{\gamma}} - 1\right)\bar{n}^2 \frac{\eta_{c_t}'}{\eta_{c_{t_{\bar{n}=1}}}'}\right)^{\frac{\gamma}{\gamma-1}} \quad (19)$$

$$\dot{m}' = \dot{m}_{\pi_{c_t}=4.5}'(-0.0249\,\pi_{c_t}'^2 + 0.4332\,\pi_{c_t}' - 0.4447) \quad (20)$$

In order to determine the variation in the compression ratio with mass flow rate at different rotating speeds, different values of the relative axial velocity higher than the surge value C_a' are used with Figs. 3 & 4. The maximum efficiency at each speed is calculated from Fig. 5. Then the resultant values are substituted in (21) & (22) to calculate the variation in both compression ratio and mass flow rate. By repeating this pro-

cess at different rotating speeds, the complete performance map is generated as shown in Fig. 6.

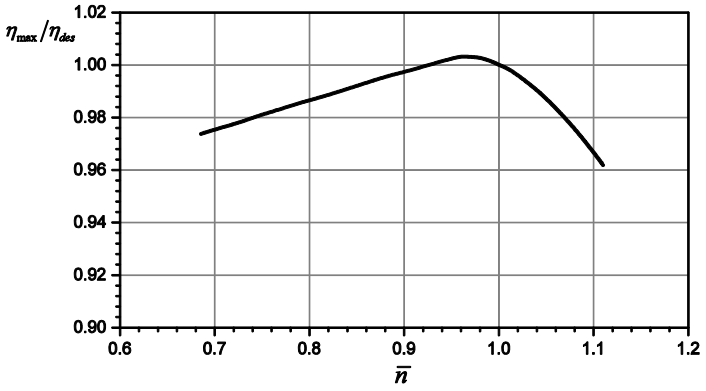

Fig. 5 Maximum compressor efficiency relative to design value, at different rotating speeds [16].

$$\pi_{c_t} = \left(1 + \frac{\pi'^{\frac{(\gamma-1)}{\gamma}}_{c_t} - 1}{\frac{w'_{c_t}}{w_{c_{t_{opt}}}} \frac{\eta'_{c_t}}{\eta_{c_{t_{max}}}}} \frac{w_{c_t}}{w_{c_{t_{opt}}}} \frac{\eta_{c_t}}{\eta_{c_{t_{max}}}}\right)^{\frac{\gamma}{\gamma-1}} \quad (21)$$

$$\dot{m} = \frac{\dot{m}'}{\hat{C}'_a} \hat{C}_a \sqrt[3]{\frac{\pi_{c_t}}{\pi'_{c_t}}} \quad (22)$$

4.2 Combustion chamber characteristics' curves

Fig. 7 represents the total pressure recovery factor across the combustion chamber, and its variation at different flow rates and temperature ratios. This map is generated using some empirical formulas [16] used to determine pressure losses in gas turbines' combustion chambers which include hydraulic losses and losses due to heat supply.

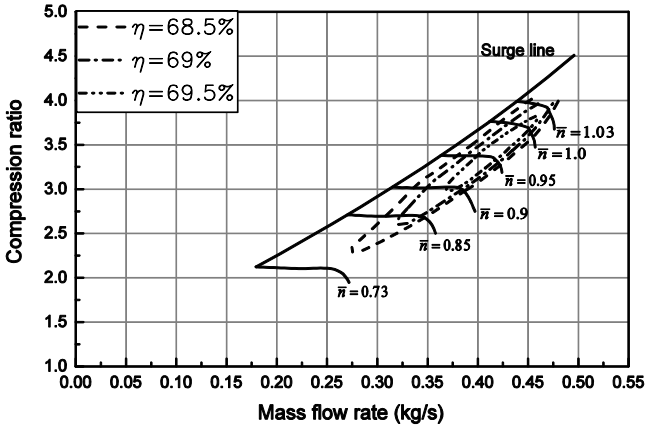

Fig. 6 Theoretical compressor performance map.

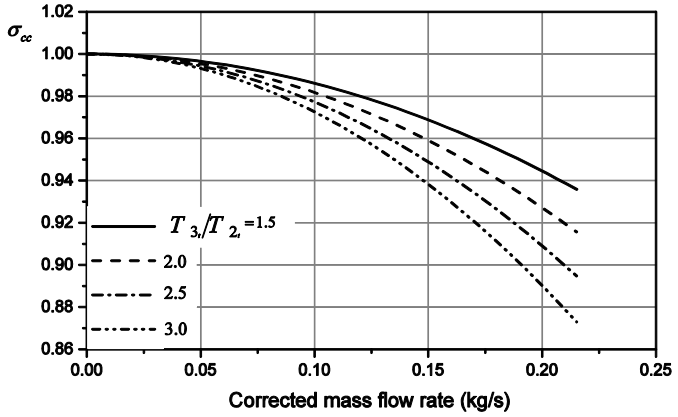

Fig. 7 Variation of total pressure recovery factor (σ_{cc}) with mass flow rate at different temperature ratios (T_{3_t}/T_{2_t}).

4.3 Turbine characteristics curve

The turbine is assumed choked on the operation range of the study; therefore, Equation (23) represents the constant choked flow rate through the turbine. This assumption is true for most of gas turbine engines for high operation speeds [16].

$$\frac{\dot{m}\sqrt{T_{3_t}}}{P_{3_t}} = constant \quad (21)$$

4.4 Nozzle characteristics curve

Basic one-dimensional gas dynamics equations [17] are used to predict the convergent nozzle performance, as shown in Fig. 8. As expected, the larger area nozzle mounted to the engine has a higher corrected mass flow rate for the same pressure ratio across the nozzle. Equation 24 represents the corrected mass flow rate through the nozzle related to the standard values of pressure and temperature.

$$\dot{m}_{corr} = \dot{m} \frac{\sqrt{\frac{T_{4_t}}{T_{stand}}}}{\frac{P_{4_t}}{P_{stand}}} \quad (22)$$

4.5 Equilibrium run curve

The ambient conditions (which defines the inlet and outlet boundary conditions of the flow across the engine) and the performance characteristics of each component of the engine are already known. In addition, three more constraints are required to achieve steady operation of the engine, which are constant flow rate through all engine components, same speed for both turbine and compressor and the turbine-generated power is just used to power the compressor and overcome mechanical losses.

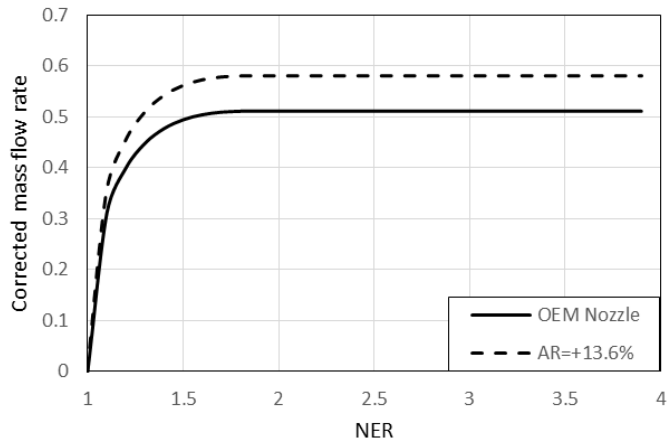

Fig. 8 Variation of corrected flow rate through the nozzle with nozzle expansion ratio ($NER = P_{4_t}/P_0$).

Solving this set of governing equations with these additional constraints and boundary conditions generates the equilibrium run curve, which describes the steady state operation of the engine at different speeds at which it does not accelerate or decelerate.

Fig. 9 shows theoretically the variation of the major engine's parameters with speed during an equilibrium run of the engine and the shift in these curves due to mounting a wider nozzle to the engine with a 13.6% larger exhaust area compared to the OEM nozzle.

5 Experimental Setup

A small test-bed is assembled in order to measure some of the engine's performance parameters. It is equipped with a load cell capable of measuring compression load up to 50 kg with accuracy of ±0.5% FS. It is used to measure the total horizontal force acting on the engine (Engine thrust). A positive displacement flow meter capable of measuring up to $100 \times 10^{-6}\ m^3/min$ of flow rate, is used to measure the fuel flow rate consumed by the engine. It has an accuracy of ±1% FS. The data from these two sensors is collected using a data acquisition capable of measuring 9.2 samples per second and has a 22-bit A/D converter.

The engine was already equipped with a RTD temperature sensor and a magnetic hall-effect rotational speed sensor. The temperature sensor accuracy is ±1% FS. The speed sensor has a resolution of 10 rpm, with no available data about its accuracy. The measured data from these two sensors is collected through the Engine Control Unit (ECU).

The load cell is calibrated using standard weights up to 24 kg and then a linear voltage/load relation is reached. The flow meter is calibrated for the fuel mixture instead of water using a known volume container and a timer. Similarly, a linear Voltage/Flowrate relation is also reached.

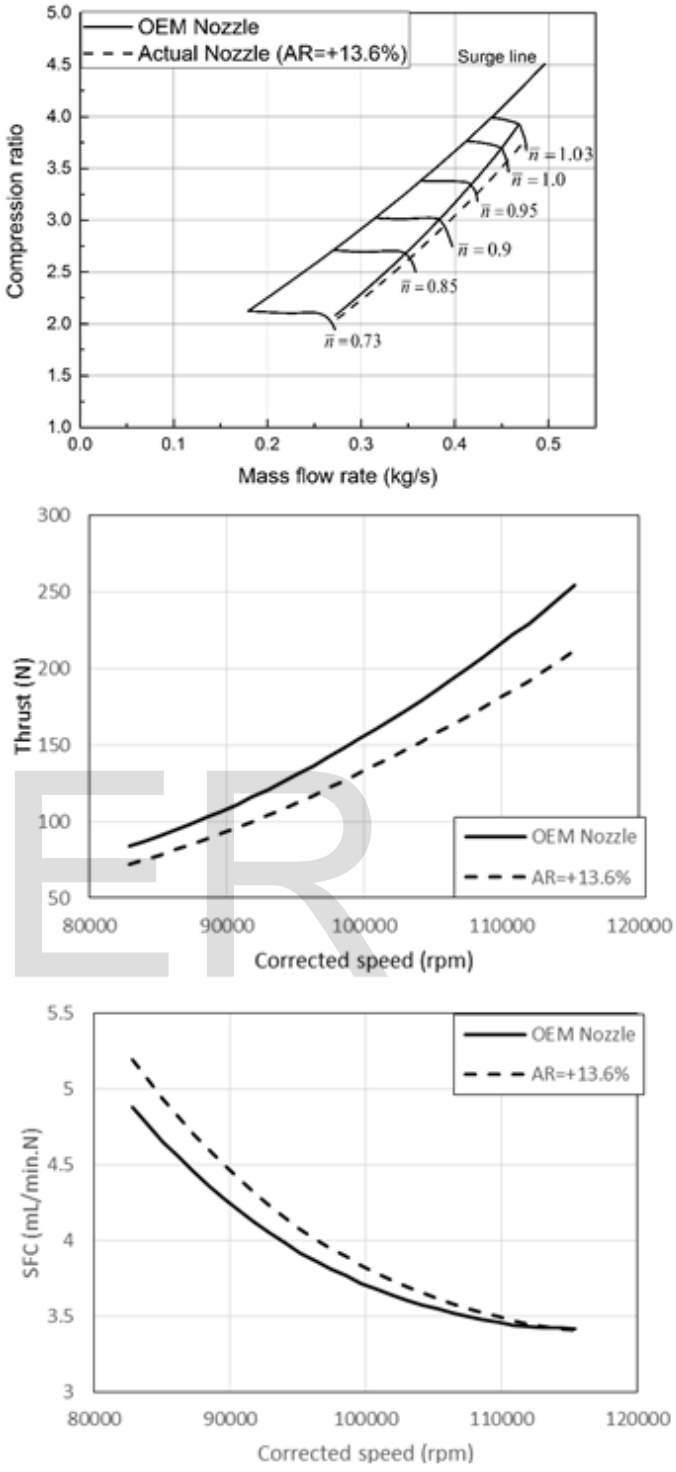

Fig. 9 Engine's parameters variation through the equilibrium run of the engine.

The engine is operated at a speed range of 33,000 to 110,000 rpm and all the pre-described parameters are recorded. These parameters are averaged at each speed after reaching a steady value. The average deviation of each parameter is summarized in Table 2.

TABLE 2 AVERAGE DEVIATION PERCENTAGE OF MEASURED PARAME-

TERS	
Thrust	1.17% to 0.23%
Fuel flow rate	0.6% to 0.76%
EGT	0.16% to 0.53%
Engine speed	0.42% to 1.45%

6 USING GASTURB SOFTWARE

The main OEM design specifications are entered as an input to the software. These data are used, in addition to standard scaled maps of a radial compressor and an axial turbine built in the program, to calculate the engine's parameters at design and off-design conditions.

A noticeable result is that it predicted the required exhaust nozzle area to achieve the stated OEM thrust of 230 N at 112,000 rpm similar to the value predicted by the model, which in both cases smaller than the actual mounted nozzle area to the engine.

7 RESULTS AND DISCUSSION

A graphical comparison between the model, GasTurb and experimental results is shown in Fig. 10. Our model underpredicted both of the thrust of the engine and its SFC with a maximum error of 10% of the actual experimental value.

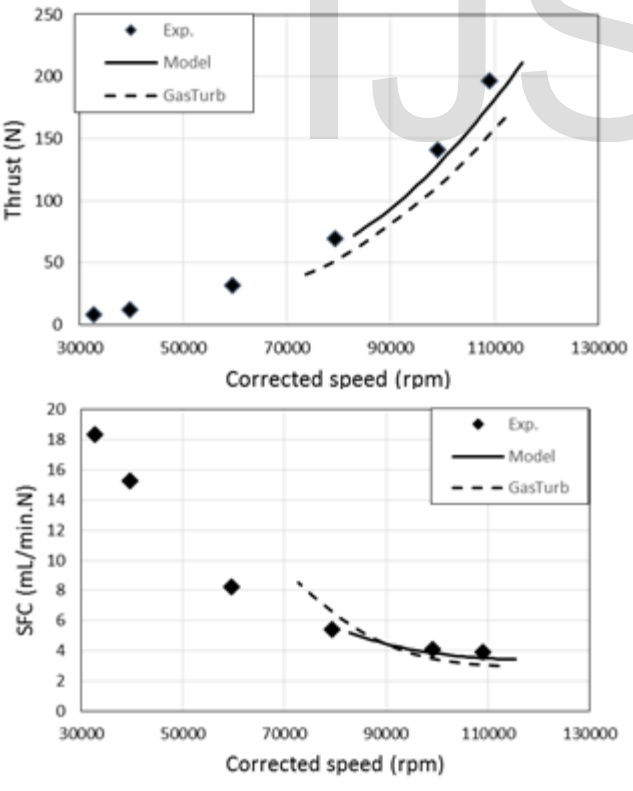

Fig. 10 Deviation of theoretical model and GasTurb from the experimental results.

The lower predicted values of the SFC is very common [2], [18] and is expected because of using a fuel mixture with 5% lubricant and part of the fuel flow is used in the lubrication of the engine's bearings. While the lower predicted thrust may be attributed to the assumption of choked turbine in this speed range and the errors arise from using empirical formulas of large-scale radial compressors to generate the compressor's map.

The GasTurb could predict the performance of the engine at larger speed range, but with larger error compared to the experimental and theoretical model. The error is more than 20% for both thrust and SFC.

8 CONCLUSION

The analytical analysis of the thermodynamic cycle combined with some empirical formulas of compressor and combustion chamber performance is found suitable for a preliminary analysis of a micro-turbojet engine performance. This theoretical model is found more accurate than the commercial software "GasTurb".

A performance map of the turbine may increase the accuracy of the model, instead of assuming it to be always choked at the studied speed range, with constant total adiabatic efficiency.

There is no available data about the speed and the temperature sensors' accuracy, which affects the experimental results. Therefore, it is recommended to replace them with more accurate and recalibrated sensors.

Until the moment, it is not possible to verify the theoretical map of both the compressor and the combustion chamber, because of the lack of temperature and pressure sensors to mount at the different stations of the engine. Therefore, it is recommended to use such sensors to verify these maps and check more precisely the ability of these empirical formulas to predict the performance of small-scale components.

NOMENCLATURE

UAV	Unmanned Aerial vehicle
SFC	Specific Fuel Consumption
CFD	Computational Fluid Dynamics
EGT	Exhaust Gas Temperature
EES	Engineering Equation Solver
y	Molar Fraction
σ	Total Pressure Recovery Factor
LHV	Lower Heating Value
OEM	Original Equipment Manufacturer
NER	Nozzle Expansion Ratio
ECU	Engine Control Unit
P	Pressure
T	Temperature
A	Area
c_p	Specific heat capacity at constant pressure
w	Specific work
η	Efficiency
C_d	Discharge coefficient
γ	Specific heat ratio
R	Specific gas constant
C	Velocity

π	Pressure ratio
$\dot{m}$	Flow rate
$\bar{n}$	Relative rotation speed

SUBSCRIPT

c	Compressor
cc	Combustion Chamber
in	Inlet
T	Turbine
t	Total or Stagnation Value
f	Fuel
a	Air
EN	Exhaust Nozzle
des	Design Value
opt	Optimum value

SUPERSCRIPT

'	Combustion Gases Property or surge properties of compressor
¯	Relative to design speed
ˆ	Relative to optimum axial velocity

REFERENCES

[1] Davison, C. R., and Birk, A. M. "Steady State and Transient Modeling of a Micro-Turbine With Comparison to Operating Engine," ASME Turbo Expo 2004: Power for Land, Sea, and Air. Vol. 6, Vienna, Austria, 2004.

[2] Leylek, Z., Anderson, W. S., Rowlinson, G., and Smith, N. "An Investigation in to Performance Modeling of a Small Gas Turbine Engine," Proceedings of ASME Turbo Expo 2013: Turbine Technical Conference and Exposition. San Antonio, Texas, USA, 2013.

[3] Mehrdad, P., Nathan, F., James, P., Eric, F., and Alireza, B. "Dynamic Modeling of a Turboshaft Engine Driving a Variable Pitch Propeller: a Decentralized Approach," 47th AIAA/ASME/SAE/ASEE Joint Propulsion Conference & Exhibit. American Institute of Aeronautics and Astronautics, 2011.

[4] Badami, M., Nuccio, P., and Signoretto, A. "Experimental and Numerical Analysis of a Small-Scale Turbojet Engine," Energy Conversion and Management Vol. 76, No. 0, 2013, pp. 225-233. doi: 10.1016/j.enconman.2013.07.043

[5] Elzahaby, A. M., Ghenaiet, A., and Elfeki, S. "Theoretical Prediction of Radial Flow Compressor Surge Line," Modeling, Measurement & Control, C, AMSE Press Vol. 41, No. 3, 1994, pp. 53-63

[6] Guo, S., Duan, F., Tang, H., Lim, S. C., and Yip, M. S. "Multi-Objective Optimization for Centrifugal Compressor of Mini Turbojet Engine," Aerospace Science and Technology Vol. 39, 2014, pp. 414-425. doi: 10.1016/j.ast.2014.04.014

[7] Gieras, M. M., and Stańkowski, T. "Computational Study of an Aerodynamic Flow through a Micro-Turbine Engine Combustor," JOURNAL OF POWER TECHNOLOGIES Vol. 92, No. 2, 2012,

[8] Benini, E., and Giacometti, S. "Design, Manufacturing and Operation of a Small Turbojet-Engine for Research Purposes," Applied Energy Vol. 84, No. 11, 2007, pp. 1102-1116. doi: 10.1016/j.apenergy.2007.05.006

[9] Pourmovahed, A., Jeruzal, C. M., and Brinker, K. D. "Development of a Jet Engine Experiment for the Energy Systems Laboratory," ASME 2003 International Mechanical Engineering Congress and Exposition, 2003. doi: 10.1115/IMECE2003-43638

[10] Davison, C. R., and Birk, A. M. "Set Up and Operational Experience With a Micro-Turbine Engine for Research and Education," ASME Turbo Expo 2004: Power for Land, Sea, and Air. Vol. 1, Vienna, Austria, 2004, p. 10.

[11] Perez-Blanco, H. "ACTIVITIES AROUND THE SR-30 MINILAB at PSU," ANNUAL CONFERENCE PROCEEDINGS - AMERICAN SOCIETY FOR ENGINEERING EDUCATION. Nashville, Tennessee, 2003.

[12] Witkowski, T., White, S., Dueñas, C. O., Strykowski, P., and Simon, T. "Characterizing the Performance of the SR-30 Turbojet Engine," American Society for Engineering Education Annual Conference & Exposition. 2003.

[13] Léonard, O., Thomas, J. P., and Borguet, S. "Ten Years of Experience With a Small Jet Engine as a Support for Education," Journal of Engineering for Gas Turbines and Power Vol. 131, No. 1, 2008, pp. 012303-012303. doi: 10.1115/1.2967487

[14] "JetCAT USA," http://www.jetcatusa.com/

[15] Çengel, Y. A., and Boles, M. A. Thermodynamics: an engineering approach: McGraw-Hill Higher Education, 2006.

[16] Elzahaby, A. M. Theory of jet engines, Printed lectures: Military technical college, MTC, Egypt, 2013.

[17] Zucker, R. D., and Biblarz, O. Fundamentals of gas dynamics: John Wiley & Sons, Inc., 2002.

[18] Bakalis, D. P., and Stamatis, A. G. "Data Analysis and Performance Model Calibration of a Small Turbojet Engine," Proceedings of the Institution of Mechanical Engineers, Part G: Journal of Aerospace Engineering Vol. 226, No. 12, 2012, pp. 1523-1533. doi: 10.1177/0954410011425126